



Article

# A Comparison between Triphenylmethyl and Triphenylsilyl Spirobifluorenyl Hosts: Synthesis, Photophysics and Performance in Phosphorescent Organic Light Emitting Diodes

Wei Wei<sup>‡ ¹</sup>, Jie Ma<sup>‡ ²</sup>, Jonas Schaab ¹, Jason Brooks ³, Seogshin Kang ¹, Matthew T. Whited ¹, Peter I. Djurovich ¹ and Mark E. Thompson ¹,²,\*

- Department of Chemistry, University of Southern California, Los Angeles, CA 90089 USA
- Mork Family Department of Chemical Engineering and Materials Science, University of Southern California, Los Angeles, CA 90089 USA
- <sup>3</sup> Universal Display Corporation, Ewing, New Jersey 08618 USA
- \* Correspondence: met@usc.edu;
- ‡ These authors contributed equally

**Abstract:** This study presents the synthesis and characterization of two spirobifluorenyl derivatives substituted with either triphenylmethyl (SB-C) or triphenylsilyl (SB-Si) moieties for use as host materials in phosphorescent organic light emitting diodes (PHOLED). Both molecules have similar high triplet energies and large energy gaps. Blue Ir(tpz)<sub>3</sub> and green Ir(ppy)<sub>3</sub> phosphorescent devices were fabricated using these materials as hosts. Surprisingly, SB-Si demonstrated superior charge transporting ability compared to SB-C, despite having similar energies for their valence orbitals. In particular, SB-Si proved to be a highly effective host for both blue and green devices, resulting in maximum efficiencies of 12.6% for the Ir(tpz)<sub>3</sub> device and 9.6% for the Ir(ppy)<sub>3</sub> device. These results highlight the benefits of the appending the triphenylsilyl moiety onto host materials and underscore the importance of considering the morphology of host in the design of efficient PHOLEDs.

Keywords: PHOLED; spirobiluorene; host morphology

**Citation:** To be added by editorial staff during production.

Academic Editor: Firstname Lastname

Received: date Revised: date Accepted: date Published: date



Copyright: © 2023 by the authors. Submitted for possible open access publication under the terms and conditions of the Creative Commons Attribution (CC BY) license (https://creativecommons.org/license s/by/4.0/).

#### 1. Introduction

Phosphorescent organic light emitting diodes (PHOLED) have been recognized as an efficient technology to achieve 100% internal efficiency in devices by harvesting both singlet and triplet excitons formed upon charge recombination.[1-3] Highly efficient and stable devices have been developed for green and red PHOLEDs. However, the performance of the blue PHOLEDs are still not comparable with its red and green counterparts, especially as the luminance efficiency for these devices degrades over long operational lifespans.[4-8] This limitation remains one of the most serious problems that needs to be addressed for widespread adoption of PHOLEDs in commercial applications.

The poor performance of blue PHOLEDs is related to properties of the host materials used in these devices. Compounds which include carbazolyl[9-12], phenylsilyl[13,14] and fluorenyl[15,16] derivatives have been widely used as hosts for PHOLEDs. However, these materials have their several disadvantages in blue PHOLEDs. Carbazolyl hosts such as (4,4'-N, N'-dicarbazole)biphenyl (CBP) and 4,4',4"-tris(carbazol-9-yl)triphenylamine (TCTA) have been reported to be unstable in blue OLEDs.[4-6] Both Scholz *et al.*[4,5] and Kondakov *at el.*[6] found that the C-N bonds between the aryl and carbazolyl groups in these hosts dissociate during device operation and produce charged or radical species.

Arylsilyl compounds have been considered as alternative host materials due to their strong Si-C bonds and they have been utilized as large band gap host materials for blue PHOLEDs.[13,14] However, the arylsilyl derivatives have poor electrical conductivity, and their deep HOMO energies (> 7.0 eV) inhibit hole injection from the hole transport layer into the emissive layer of the devices. Fluorenylsilanes,[15,16] which have both higher HOMO levels (6.6 eV) and charge mobilities, were developed later for use in blue PHOLEDs, but the large barrier for hole injection still leads to a low device efficiency.

Spirobifluorenyl derivatives have also been used as host materials in PHOLEDs as they are reported to exhibit higher glass transition temperatures compared to the fluorenyl moieties.<sup>13</sup> Spirobifluorenyl species also have much higher hole mobilities than fluorenyl derivatives although the latter have slightly higher electron mobilities.<sup>14</sup> As mentioned previously the deep HOMO energy of the fluorenes (6.2 eV - 6.6 eV) could impede hole injection in blue OLEDs. Considering the similar HOMO levels of the spirobifluorenes, the greater hole carrier mobility of this species may improve the charge balance in the OLED devices. Several spirobifluorenyl-based hosts have been reported to achieve good thermal stability and avoid labile heteroatom linkages such as C-S, C-P or C-N by adding aromatic groups such as phenyl, triphenyl, or spirobifluorenyl into the spirobifluorene backbone.[17-19] However, due to negligible steric hindrance between the moieties, these hosts have lower triplet energies compared to spirobifluorene (E<sub>T</sub> = 2.8 eV) and therefore are poor candidates for confining triplet excitons on blue phosphorescent dopants in PHOLEDs. To address this issue, highly twisted spirobifluorenyl dimers and oligomers with an ortho-ortho linkage between spirobifluorenes moieties were introduced by Ma and Poriel et al., [20-24] which inhibited conjugation and retained the high triplet energy of the parent spirofluorene.

In this study, a design strategy was utilized to maintain high triplet energy in spirobifluorenyl-based hosts and compare two different derivatives by introducing a tetravalent atom to isolate pendant phenyl rings. Specifically, a non-conjugated carbon core based triphenylmethyl spirobifluorenyl compound, SB-C (Scheme 1), and its triphenylsilyl analog, SB-Si (Scheme 2), were synthesized. Various studies were conducted to compare the properties of these host materials, and their performance was evaluated in blue and green phosphorescent organic light-emitting diodes (PHOLEDs). Some of the results presented here appeared in one of the authors' (Wei Wei) PhD thesis.[25]

2. Results

#### 2.1. Synthesis

Both of SB-C and SB-Si were designed to maintain high singlet and triplet energies by using the pendant C or Si to isolate the aromatic groups of these two moieties. These two materials were synthesized using different synthetic methodologies starting from a common 2-bromo-9, 9'-spirobifluorene (1) precursor. The synthesis of SB-C follows a four-step synthetic route as shown in Scheme 1. A Grignard reagent prepared from 1 was treated with benzophenone to produce the diphenyl-9,9-spirobifluoren-2-yl methanol (2). A Friedel-Crafts reaction between 2 and aniline under a strong acidic condition afforded the p-(diphenyl-9,9-spirobifluoren-2-yl)methyl aniline (3). The amino group of 3 was then removed using tBuONO and H<sub>3</sub>PO<sub>2</sub> to give the final product (SB-C). The overall yield of this multi-step synthesis is 33%. SB-Si was synthesized more efficiently as shown in Scheme 2. Addition of Ph<sub>3</sub>SiCl to 2-lithio-9,9'-spirobifluorene gives the SB-Si with a yield of 78% as a pure isolated product.[23,24]

Scheme 1. Synthesis of SB-C

Scheme 2. Synthesis of SB-Si

#### 2.2. X-ray Structures

X-ray crystal structures for Sb-C and SB-Si were obtained and are shown in Fig. 1. The bond distance between the spirobifluorenyl carbon and the triphenylmethyl carbon center in SB-C (C1-C20 = 1.547 Å) is shorter than for the equivalent bond in SB-Si (Si1-C19 = 1.873 Å), as are the bond distances between the sp<sup>3</sup> center to the atoms on the phenyl rings (C1-C<sub>Ph</sub> = 1.548-1.554 Å for SB-C and Si1-C<sub>Ph</sub> = 1.874-1.880 Å for SB-Si). The packing of the molecules in a unit cell of each of the materials is shown in Fig. S1. No overlap of the aromatic rings is found for SB-C, whereas partial overlap was observed in SB-Si. However, it is worth noting that the shortest full face-to-face distance in SB-Si is approximately 5 Å, which is too long to be effective for  $\pi$ - $\pi$  stacking interactions.

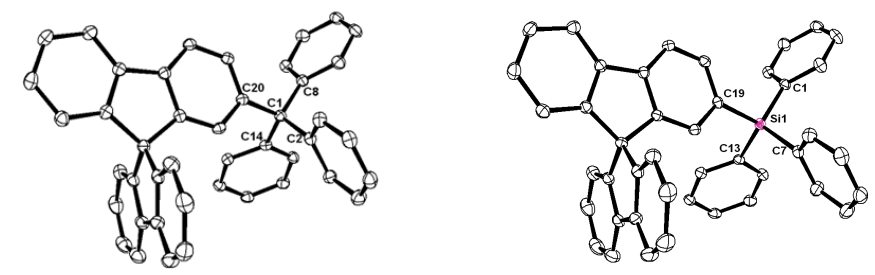


Figure 1. X-ray crystal structures of SB-C (left) and SB-Si (right)

#### 2.3. Theoretical Calculations

In order to quantitate other intermolecular interactions, Hirshfeld surface calculations were applied in conjugation with the X-ray data to explore the interatomic distances of these two materials. A Hirshfeld surface identifies regions where the intermolecular interactions of a molecule in the crystal lattice are shorter than a boundary defined by a

90

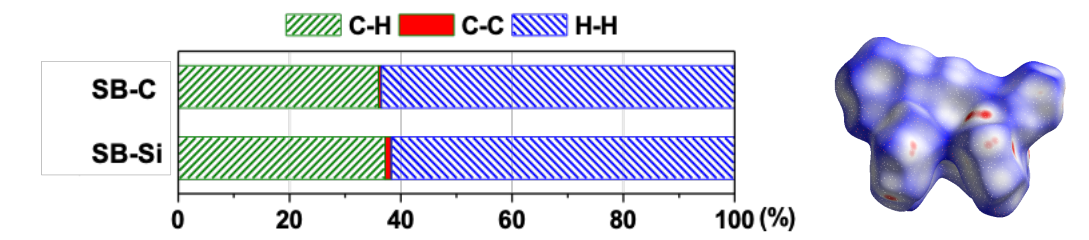
93 94 95

96

> 105 106

107 108 109

hypothetical Van der Waals surface calculated for the isolated molecule. [26] Areas of the molecules where the intermolecular interactions are closer can be quantified and compared to other regions where interactions are longer (Fig. S2). The fingerprint generated from the Hirshfeld surface can then provide detailed information regarding the types and percentages of these interactions. Crystalline SB-Si shows higher ratios of both C···C and C···H type interactions between molecules than found in SB-C, which instead has a higher ratio of H···H type intermolecular interactions (Fig. 2). Density functional theory (DFT) calculations also determined the energies for the highest occupied and lowest unoccupied molecular orbitals (HOMO and LUMO) of the two molecules (Fig. S3). These two molecules have similar HOMO and LUMO surfaces. The HOMO is delocalized across the entire spirobifluorenyl moiety whereas the LUMO is localized on the fluorenyl linkage substituted to the Ph<sub>3</sub>C- or Ph<sub>3</sub>Si- groups. The calculated HOMO and LUMO levels for both molecules are -5.6 eV and -1.0 eV, respectively.



	CH (%)	CC (%)	HH (%)
SB-C	36.0	0.5	63.5
SB-Si	37.2	1.1	61.7

**Figure 2.** Intermolecular interactions between molecules in SB-C and SB-Si crystals calculated using Crystal Explorer software package. Different colors indicate different types of close intermolecular interactions (C···H, C···C or H···H). The x-axis shows the percentage of each interaction and is tabulated below. An illustration of a Hirshfeld surface for SB-C is shown on the right.

#### 2.4. Electrochemistry

The electrochemical properties of SB-C and SB-Si were examined using cyclic voltammetry (CV) and differential pulse voltammetry (DPV) (Table 1 and Fig. S4). Electrochemical reversibility was established using CV measurements whereas the redox potentials were determined using DPV and referenced to an internal ferrocenium/ferrocene couple. Both compounds are oxidized irreversibly at ca. 1.3 V. Similar irreversible oxidation potentials have been reported for the parent spirobifluorene and its non-conjugated derivatives.[27,28] A second irreversible oxidation wave was also observed at 1.7 V for both SB-C and SB-Si (Fig. S4a). These two waves are similar to oxidative processes that have been reported for other spirobifluorenes.[27,28] The first oxidation wave was thus assigned to oxidation of the fluorenyl moiety bound to the CPh<sub>3</sub> or SiPh<sub>3</sub> group, whereas the second wave is assigned to oxidation and polymerization of the unsubstituted fluorenyl moiety. The reduction waves for SB-C and SB-Si are also irreversible and were detected near the edge of the solvent window at -3.0 V for SB-C and -2.8 V for SB-Si (Table 1, Fig. S4a). Energy levels for the HOMO and LUMO were estimated from the electrochemical data of these two molecules using correlations between the redox potentials. The HOMO levels are -6.2 and -6.3 eV for SB-C and SB-Si, respectively, whereas the LUMO levels are -1.3 eV for the SB-C and -1.5 eV for the SB-Si. The HOMO energies are similar to the value reported for SB-Si (-6.2 eV) obtained using photoemission yield spectroscopy.[24] Moreover, the oxidation potential observed for SB-Si (1.34 V) is close to values reported for a series of silicon substituted dimethylfluorenyl compounds ( $E_{\text{ox}} = 1.4$ 

V).[16,29] The transport gaps calculated from the difference of the HOMO and LUMO levels are 4.9 eV and 4.8 eV for SB-C and SB-Si, respectively. Hence, the large energy gaps of SB-C and SB-Si are comparable to their fluorenyl counterparts which make them promising candidates for hosting blue dopants.

**Table 1.** Electrochemical data. Measurements were performed using 0.1 M TBAPF6 electrolyte, and the potentials are listed relative to a ferrocene internal reference.

	$E_{ox^a}(V)$	E <sub>red</sub> <sup>b</sup> (V)	HOMO <sup>c</sup> (eV)	LUMOc (eV)
SB-C	1.25	-3.00	-6.2	-1.3
SB-Si	1.34	-2.82	-6.3	-1.5

<sup>a</sup> In acetonitrile; <sup>b</sup>in DMF; <sup>c</sup> calculated using the equations HOMO = -1.15 ( $E_{ox}$ ) - 4.79; LUMO = -1.18 ( $E_{red}$ ) - 4.83 according to reference [30].

#### 2.5. Thermal Properties

The glass transition temperatures ( $T_g$ ) of the materials are considered to be an important factor for obtaining homogenous thin films in OLED devices.[31-34] Due to the steric bulk of the spirobifluorenyl substituent, a high glass transition temperature 87 °C was observed for SB-Si (Table 2 and Fig. S5). In contrast, we were not able to detect the glass transition temperature of SB-C. The melting temperature of SB-C ( $T_m = 284$  °C) is also higher than that of SB-Si ( $T_m = 253$  °C) (Table 2 and Fig. S5). The sublimation temperatures of these two molecules are not influenced by either the C or the Si center and both compounds can be sublimed at 245 °C in high yield (80-90%) using a gradient vacuum sublimator. This makes these two molecules suitable for OLED device fabrication using vapor deposition methods.

Table 2. DSC data

	Tm (°C)	T <sub>g</sub> (°C)	T <sub>sub</sub> (°C)
SB-C	284	-	245
SB-Si	253	87	245

#### 2.6. Photophysics

The UV-visible absorption and photoluminescence (PL) spectra of SB-C and SB-Si in 2-methyltetrahydrofuran (2-MeTHF) solutions are shown in Fig. 3a. Absorption bands appearing between 290 nm to 320 nm are attributed to  $\pi$ - $\pi$  transitions on the spirobifluorene.[35,36] The lowest energy transitions of both molecules are at 315 nm (Table 3). The optical gaps determined from the long wavelength edge of the absorption spectra are near identical for the SB-C ( $\lambda$  = 317 nm, 3.9 eV) and the SB-Si ( $\lambda$  = 316 nm, 3.9 eV). These optical gaps are ~ 1 eV smaller than the transport gaps determined from their respective redox potentials. Singlet emission typical for the fluorenyl moiety was observed from SB-C ( $\lambda$ max = 320 nm) and SB-Si ( $\lambda$ max = 318 nm) (Table 3 and Fig. 3a). The phosphorescence spectra of SB-C ( $\lambda$ max = 443 nm) and SB-Si ( $\lambda$ max = 438 nm) were observed at low temperature (77 K gated), Table 3 and Fig. 3a (inset). The triplet energies for both molecules (E<sub>T</sub> = 2.80 eV) are only slightly lower compared to the parent fluorenylsilanes ( $\lambda$ max = 435 nm, E<sub>T</sub> = 2.85 eV).[16]

192 193

194

195

196

197

198

199

200

201

202

203

204

205

206

207

208

209

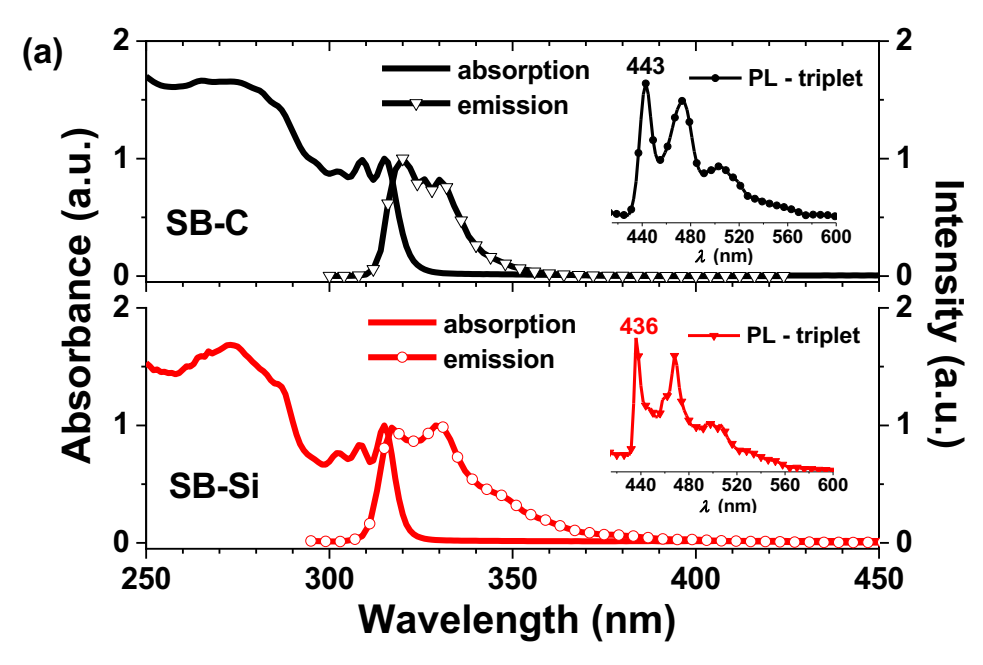


Figure 3a. Absorption and emission spectra of SB-C and SB-Si in 2-MeTHF solution.

The excitation and emission spectra of crystals of SB-C and SB-Si were also measured so a direct correlation with their molecular arrangements in their solid-state could be made using the X-ray and photophysical data (Fig. 3b). The excitation spectrum of SB-C crystals shows a maximum peak at 314 nm, which is 3 nm blue shifted from its solution absorption. A 36 nm red shift was also observed for the emission spectrum of crystalline SB-C from its spectrum in solution. In contrast, the excitation spectrum of SB-Si crystals shows a strong red shift (47 nm) from to its solution absorption, giving a maximum excitation at 362 nm (Table 3, Fig. 3b). Associated with the red shift of the excitation, the emission of this compound is also red shifted for 59 nm from its emission in solution. The red shifted emission spectra of SB-C and SB-Si come from the intermolecular interactions between molecules in the crystals. The large red shifts of both excitation and emission spectra of SB-Si suggest that a greater number of close intermolecular interactions are present in the crystals than in SB-C. The Hirshfeld surface calculation discussed in the previous section also provides evidence of stronger intermolecular, C···C type interactions are present in the SB-Si crystals. However, similar phosphorescence spectra for SB-C and SB-Si  $(\lambda_{\text{max}} = 450 \text{ nm})$  were observed at 77K for both compounds (Table 3, Fig. 3b inset).

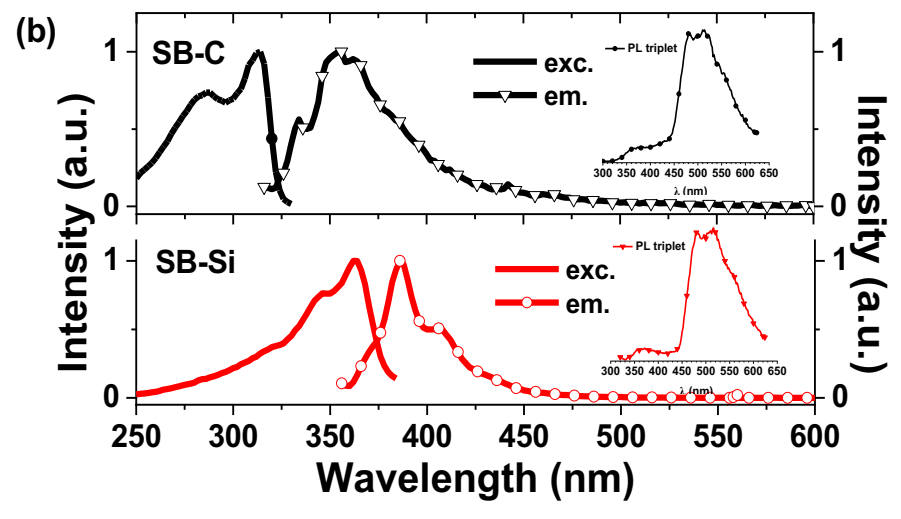
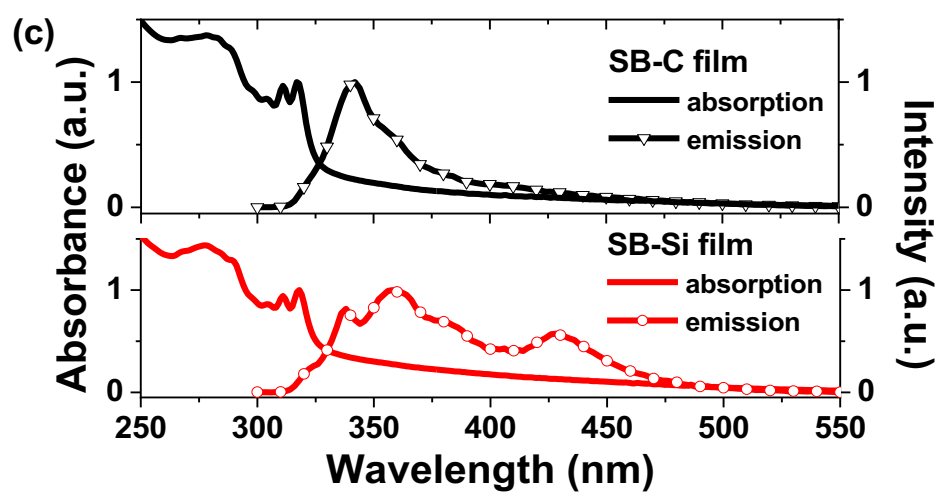


Figure 3b. Excitation and emission spectra of SB-C and SB-Si from sublimed crystals.

It is particularly important to investigate the photophysics of SB-C and SB-Si in amorphous thin films, since these two materials were designed for thin film semiconductor devices. Therefore, absorption and emission spectra of vacuum deposited thin film were measured and are shown in Fig. 3c. The lowest energy absorption transitions appear at 318 nm for both materials and are close to values measured in dilute solution. The gradually sloping absorption band after 330 nm is due to light scattering. Even though films of these two compounds have similar absorption spectra, their emission spectra are quite different. Emission from the SB-C film peaks at 342 nm, whereas two different red shifted bands in SB-Si peak at 360 nm and 430 nm. The bands between 330 and 400 nm are assigned to be singlet emission from the molecules that are red shifted in the solid state. The red shift could be due to weak interactions between molecules in the films, considering that there are no interactions between individual molecules in a dilute solution. The emission band at 430 nm in SB-Si is similar to emission observed from solid films of dimethylfluorenyl silanes[16] and has been assigned to fluorescence from more strongly aggregated molecules which act as luminescent trap states.



**Figure 3c.** Absorption and photoluminescence (PL) spectra of SB-C and SB-Si from amorphous thin films (40 nm).

**Table 3.** Summary of photophysical data

	$\lambda_{ m Abs}^a$ (nm)	$\lambda_{ ext{PL}^a}$ (nm)	$\lambda_{ ext{PL,77K}^a}$ (nm)	$\lambda_{\mathrm{Exc,  crystal}}^{\mathrm{b}}$ (nm)	λ <sub>PL, crystal</sub> <sup>b</sup> (nm)	λΡL, 77K crystal <sup>b</sup> (nm)	$\lambda_{Abs, film}^{c}$ (nm)	λ <sub>PL, film</sub> c (nm)
SB-C	315	320	443	314	356	480	317	342
SB-Si	315	318	436	362	386	480	318	360, 430

<sup>&</sup>lt;sup>a</sup>In 2-MeTHF; <sup>b</sup>sublimed crystals; <sup>c</sup> amorphous thin film (40 nm)

#### 2.7. OLED studies

The charge transport properties of SB-C and SB-Si were evaluated by comparing the performance of undoped OLED devices fabricated with the structure: ITO/NPD (30 nm)/mCP (10 nm)/SB-C or -Si host (20 nm)/Alq³ (20 nm) /LiF (1 nm) /Al (100 nm) (Fig. S6). The electroluminescence (EL) spectra of each host are voltage dependent in the range 8 V–15 V for both SB-C and SB-Si (Fig. S6). With increasing voltage, emission from NPD increases whereas emission from Alq³ decreases. However, the SB-C device gives predominant emission from NPD in the whole range examined potentials, whereas the SB-Si device displays predominant emission from Alq³ (Fig. 4a). Since these two materials have similar HOMO and LUMO energies, the devices should have similar charge injection barrier for holes and electrons. Thus, the different EL spectra of these two materials may come about from the difference in the carrier mobilities in the two materials. The current voltage

246

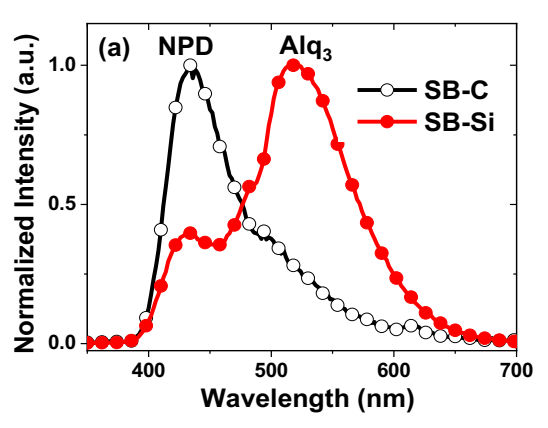
247

248

249

250

(*J-V*) characteristics of these two devices are shown in Fig. 4b. A larger current was observed for the SB-Si device at high voltage. This difference could be because the SB-Si film has a higher percentage of aromatics rings in close enough proximity to facilitate charge transfer than does SB-C. This is consistent with the Hirshfeld surface calculations, which suggest that SB-Si has a larger proportion of C···C intermolecular interactions in the crystalline state than SB-C.



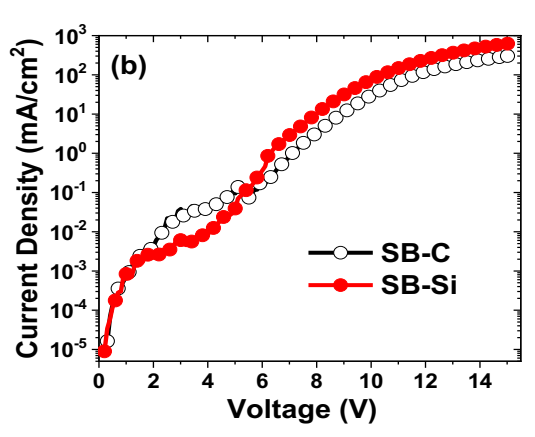


**Figure 4.** (a) EL spectra at 9 V and (b) *J-V* plot of undoped SB-C and SB-Si devices.

Phosphorescent devices using the green emissive dopant tris(2-phenylpyridyl)iridium(III) Ir(ppy)3 were fabricated to investigate the properties of two hosts in PHOLEDs. The device structure chosen for these devices was: ITO / HATCN (10 nm)/ NPD (30 nm) / (9% Ir(ppy)3: SB-C or -Si host (30 nm) / BAlq (10 nm)/ Alq3 (40 nm)/ LiF (1 nm) /Al (100 nm), using hexaazatriphenylenehexacarbonitrile (HATCN) as a hole injection material and bis(2-methyl-8-quinolinolato-N,O)-(1,1'-biphenyl-4-olato)aluminum (BAlq) as a hole blocking material. It was necessary to dope Ir(ppy)3 at a high level in these devices as the dopant must carry both hole and electrons due to the wide energy bandgap of the host. The performance of these two devices is summarized in Table 4. The EL spectra of these two devices are shown in Fig. 5a. Both devices achieve good charge balance at the emissive layer, leading to pure Ir(ppy)3 emission at 511 nm. The current density-voltage-luminance (J-L-V) characteristics of these two devices are shown in Fig. 5b and 5c. A higher current density and brightness is found at all voltages for the SB-Si device than for the SB-C device. Correspondingly, the SB-Si device turns on at a lower voltage ( $V_{\text{turn-on}} = 3.9 \text{ V}$ ) than the SB-C device (V<sub>turn-on</sub> = 5.2 V). The device with the SB-Si host shows a maximum external quantum efficiency (EQE) of 9.6 % at a current density of 4.24 mA/cm<sup>2</sup>, whereas the maximum EQE of the SB-C device is only 1.2 % (Fig.5d). Ir(ppy)3 is prone to aggregation at these high doping concentrations which leads to lower efficiency for the devices. Therefore, these Ir(ppy)3 devices provide a good measure of the ability of the host material to disperse the dopant. The high performance of the SB-Si device shows that this material is significantly better at dispersing Ir(ppy)3 than SB-C. The EQE obtained using SB-Si also agrees with data from previous published OLED devices using Ir-based emitters in the same SB-Si host.[23,24]

263

264

265

266

267

268

270

271

272

273

274

275

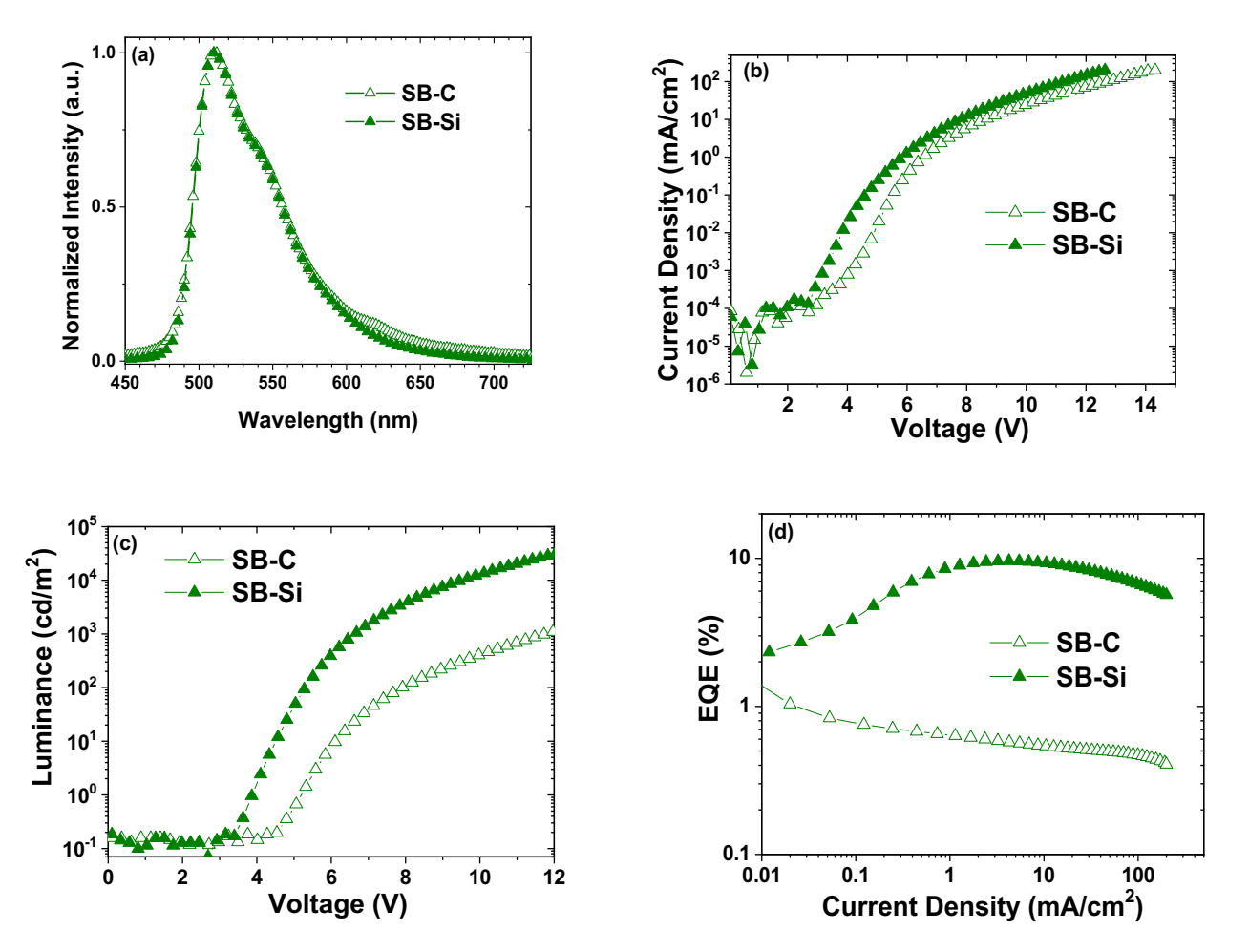


**Figure 5.** OLED device characteristics of  $Ir(ppy)_3$  devices. (a) EL spectra (b) J-V (c) L-V, and (d) EQE-current density plots.

The two hosts materials were also examined in blue PHOLED devices using tris(N,N-di-p-tolyl-pyrazinoimidazol-2-yl)iridium(III) (Ir(tpz)3) as the phosphorescent emitter.[37] A doping weight percentage of 20% was determined to be optimal for these devices and host materials, as other concentrations showed a worse performance. To see the difference in a sky-blue material, which is not as prone to aggregation as Ir(ppy)3, and to compare SB-Si with SB-C, the following device structure was used: ITO / HATCN (5 nm) / TAPC (40 nm) / SB-C or -Si (10 nm) / (20% Ir(tpz)<sub>3</sub> : SB-C or -Si host, 25 nm) / BP4mPY (60 nm) / LiF (1 nm)/ Al (100 nm). The performance of these two devices is summarized in Table 4. Here di-[4-(N,N-di-p-tolyl-amino)-phenyl]cyclohexane (TAPC) was used as a hole transporting layer, 3,3',5,5'-tetra[(m-pyridyl)-phen-3-yl]biphenyl (BP4mPY) was used as an electron transporting layer, and 10 nm undoped host was used as an electron blocking layer. Electroluminescence only from Ir(tpz)3 was observed for both SB-C and SB-Si devices (Fig. 6a). The SB-Si device exhibits higher current conduction and luminance than the SB-C device at any given voltage (Fig 6b and 6c). For example, at 4 V the SB-C device gives a current density of 17.8 mA/cm<sup>2</sup> and a luminance of 1200 cd/m<sup>2</sup>, whereas the SB-Si device reaches two times larger current (35 mA/cm<sup>2</sup>) and five times higher luminance (6300 cd/m<sup>2</sup>). The SB-C device reaches its highest efficiency (EQE = 10.2%) with a current density of 0.01 mA/cm<sup>2</sup> (Fig. 6d). A significant decrease of the external efficiency was observed in the SB-C device starting from a current density of 0.7 mA/cm<sup>2</sup>, which could be due to triplet-triplet annihilation. The SB-Si device reaches its maximum external quantum efficiency (12.6 %) at current of 1 mA/cm<sup>2</sup> and no significant drop in EQE was observed for this device until the current density increased to 10 mA/cm<sup>2</sup>

277

300

(a)

SB-C SB-Si

Normalized Intensity (a.u.)

0.5

400

(c)

10<sup>5</sup>

10<sup>4</sup>

10<sup>3</sup>

10<sup>2</sup>

10<sup>1</sup>

10<sup>0</sup>

Luminescence (cd/m<sup>2</sup>)

450

500

SB-C

SB-Si

550

Wavelength (nm)

600

5

Voltage (V)

6

650

700

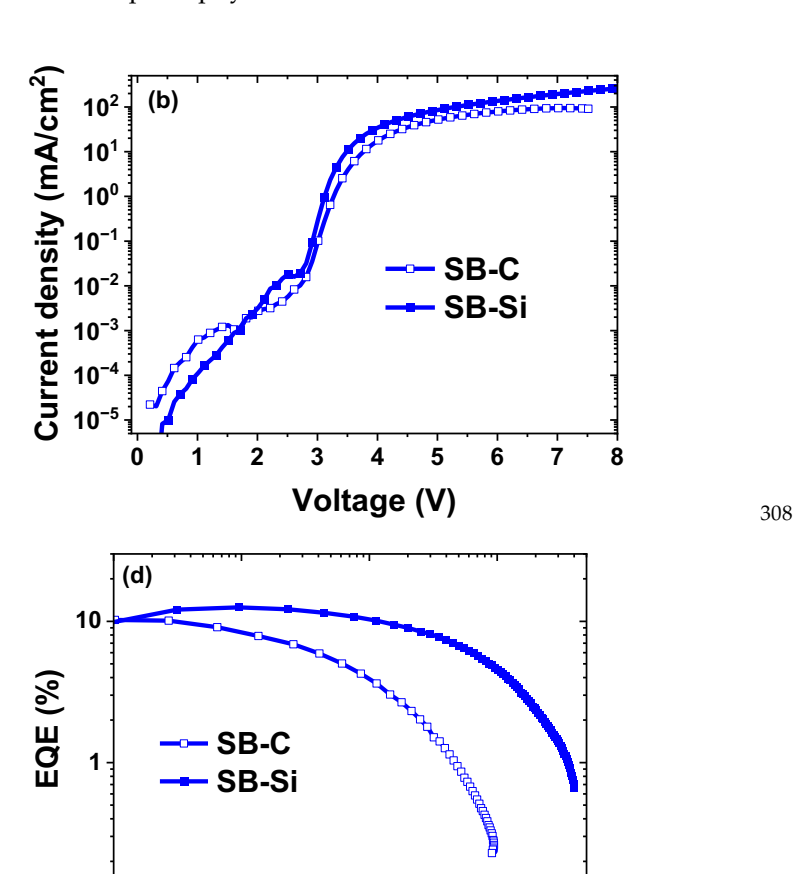
304

305

306

307

(Fig. 6d). Overall, devices using the SB-Si host exhibited superior conductivity, higher luminance and enhanced EQE at any given voltage over devices using the SB-C host. These improvements can be attributed to the increased intermolecular C···C interactions in SB-Si, as suggested by the calculated and photophysical data.



10

Current density (mA/cm<sup>2</sup>)

100

**Figure 6.** OLED device characteristics of  $Ir(tpz)_3$  devices. (a) EL spectra (b) J-V (c) L-V, and (d) EQE-current density plots.

0.1 <del>↓</del> 0.1

Table 4. Summary of OLED performance.

			@ 1000 c	d m <sup>-2</sup>	
EML	$V_{ m turn ext{-}on}$ a $({ m V})$	EQE <sub>max</sub> (%)	EQE (%)	J (mA/cm <sup>2</sup> )	$\lambda_{\max}$ (nm), CIE
		ı	9 wt% Ir(ppy)3		
SB-C	5.2	1.2	0.6	61.9	511, (0.28,0.61)
SB-Si	3.9	9.6	9.6	3.2	512, (0.28,0.63)
		,	20 wt% Ir(tpz)3		
SB-C	2.8	10.2	3.6	11.4	488, (0.26,0.54)
SB-Si	2.8	12.6	11.7	4.4	483, (0.20,0.43)

309 310 311

312313

#### 3. Materials and Methods

#### 3.1. Synthesis

All chemicals and solvents were purchased from commercial sources without further purification except for tetrahydrofuran (THF) that had been distilled over sodium/benzophenone.

Triphenyl-9,9-spirobifluoren-2-yl silane (SB-Si).[23,24] To a solution of 0.78 g (2 mmol) 2-bromo-9,9-spirobifluorene (1) in dry THF was added 1.38 ml (2.2 mmol) n-BuLi (1.6 M in hexanes) under N2 atmosphere to get an orange solution. Triphenylchlorosilane (0.56 g, 1.9 mmol) was initially weighed and dissolved in THF under N2 atmosphere and was added using syringe into the solution after 1 hour. The solution was stirred overnight. Ethyl acetate and water were used to extract the organic layer, which was later dried over brine and magnesium sulfate. Organic solvents were reduced by rotary evaporation to obtain an orange colored solid which was recrystallized in CH2Cl2 to get 0.89 g white solid of the product.

Triphenyl-9,9-spirobifluoren-2-yl methane (SB-C). A solution of 1.74 g 1 was added dropwise to Mg in 8 ml THF. A solution of benzylphenone in 4 ml THF was slowly added into the prepared Grignard reagent at room temperature and the mixture was refluxed for three hours. After cooled down to the room temperature, ammonium chloride was used to quench the reaction. The organic layer was extracted by CH2Cl2 and dried over MgSO4. After the solvent was removed using rotary evaporation, a silica gel column with CH<sub>2</sub>Cl<sub>2</sub>/hexanes (1:3) was performed to give 1.63 white solids of diphenyl-spirobifluorenyl methanol (2), Yield: 81%. Compound 2 (3.17 mmol, 1.58 g) was refluxed with aniline (4.8 mmol, 0.44 ml), HCl (0.5 ml) and acetic acid (10 ml) at 140 °C for 3 days. The reaction mixture was allowed to cool down to the room temperature and 100 ml water was added. NaOH solid was added until the solution becomes neutral. The product was filtered out as 1.65 g white solids of diphenylspirobifluorenylaniline methane (3). To a solution of 0.57 g of 3 in 30 ml THF, a solution of 6 mmol H<sub>3</sub>PO<sub>2</sub> in H<sub>2</sub>O (0.5 ml) was added. After stirring for 10 mins, a solution of tBuONO in 5 ml THF was added and the mixture was stirred for 16 h at 40 °C. After the THF was removed, the reaction mixture was extracted by CH<sub>2</sub>Cl<sub>2</sub> and water. The organic layer was washed by brine and dried over MgSO<sub>4</sub>. After the solvent was removed with reduced pressure, recrystallization was performed to give 2.51 g white solids of the product.

<sup>1</sup>H NMR, mass spectrometry and elemental analysis data of these compounds are shown as follows:

*Triphenyl-9,9-spirobifluoren-2-yl silane* (**SB-Si**) Yield: 78%. ¹H NMR (CDCl₃, 250 Hz): δ 7.80 -7.87 (2H, dd, Ar-H), 7.74-7.78 (2H, d, Ar-H), 7.45-7.49 (1H, d, Ar-H), 7.29-7.41 (12H, m, Ar-H), 7.20-7.27 (5H, m, Ar-H), 7.08-7.15 (4H, dd, Ar-H), 7.05 (1H, s, Ar-H), 6.75 − 6.79 (2H, d, Ar-H), 6.71-6.75 (1H, d, Ar-H). MS (m/z): 574, 497, 316, 259. Ana. Calcd. for C₄₃H₃₀Si: C 89.85 H 5.26; Found: C 90.07 H 5.12.

Diphenyl-9,9-spirobifluoren-2-yl methanol (2), Yield: 81%. ¹H NMR (CDCl₃, 400 Hz) δ: 7.79 -7.81 (1H, d, Ar-H), 7.77-7.79 (2H, d, Ar-H), 7.69-7.71 (1H, d, Ar-H), 7.33-7.38 (1H, d, Ar-H), 7.31-7.36 (2H,dd, Ar-H), 7.18-7.22 (4H, d, Ar-H), 7.18-7.21 (2H, dd, Ar-H), 7.12-7.17 (4H, dd, Ar-H), 7.04-7.10 (1H, dd, Ar-H), 6.92 (1H, s, Ar-H), 6.72-6.75 (2H, d, Ar-H), 6.67-6.70 (1H, d, Ar-H). MS (m/z): 498, 482, 421, 315.

*p-(Diphenyl-9,9-spirobifluoren-2-yl)methyl aniline* (3), Yield: 91%. <sup>1</sup>H NMR (CDCl<sub>3</sub>, 250 Hz): δ 7.75-7.79 (1H, d, Ar-H) 7.69 -7.73 (2H, d, Ar-H), 7.25 -7.32 (3H, m, Ar-H), 7.21-7.24 (1H, d, Ar-H), 7.01-7.10 (11H, m, Ar-H), 6.80-6.83 (2H, d, Ar-H), 6.68-6.71 (2H, d, Ar-H), 6.65 -6.68 (1H, d, Ar-H), 6.56-6.58 (1H, s, Ar-H), 6.40-6.43 (2H, d, Ar-H). MS (m/z): 572, 481, 258.

*Triphenyl-9,9-spirobifluoren-2-yl methane* (**SB-C**), Yield: 45%. <sup>1</sup>H NMR (CDCl<sub>3</sub>, 400 Hz) 5: 7.76 -7.79 (1H, d, Ar-H), 7.71-7.73 (2H, dd, Ar-H), 7.68-7.70 (1H, d, Ar-H), 7.30-7.34 (1H, dd, Ar-H), 7.27-7.31 (2H, dd, Ar-H), 7.23-7.26 (1H, d, Ar-H), 7.03-7.12 (18H, m, Ar-H), 6.68

-6.70 (2H, d, Ar-H), 6.62-6.68 (1H, d, Ar-H), 6.55 (1H, s, Ar-H). MS (m/z): 558, 481, 403, 316. Ana. Calcd. for C<sub>44</sub>H<sub>30</sub>: C 94.59 H 5.41; Found: C 94.45; H 5.31.

#### 3.2. X-ray Crystallography

X-ray quality crystals were grown as indicated in the experimental procedures for each complex, and the crystals were mounted on a nylon fiber with Paratone-N oil. All crystals were measured at 100K with a Rigaku Xta LAB Synergy S, equipped with an HyPix-600HE detector and an Oxford Cryostream 800 low temperature unit, using Cu K $\alpha$  PhotonJet-S X-ray source. The frames were integrated using the SAINT algorithm to give the hkl files. Data were corrected for absorption effects using the multi-scan method (SA-DABS) with Rigaku CrysalisPro. The structures were solved by intrinsic phasing and refined with the SHELXTL software package.4. Structures of SB-C and SB-Si were deposited in the CCDC (2221201 and 2216982, respectively).

#### 3.3. Thermal Analysis

Differential Scanning Calorimetry (DSC) was performed on a TA Instruments DSC Q10 instrument with a scanning range from room temperature to 300 °C. The sample was first scanned at a heating rate of 10 °C min<sup>-1</sup> and was cooled down to room temperature rapidly using liquid  $N_2$ . The second and third scans were performed at a heating rate of 5 °C min<sup>-1</sup>. The glass transition temperatures were determined from either the second or the third scan for each compound.

#### 3.4 Electrochemistry and Photochemistry

Cyclic voltammetry was performed using an EG&G potentiostat/galvanostat model 283 under  $N_2$  atmosphere. A glass carbon rod was used as the working electrode. Tetrabutylammonium hexafluorophosphate (TBAPF6, 0.1 M) was used as the supporting electrolyte. Anhydrous acetonitrile was used as the solvent for the oxidation measurements and anhydrous DMF was used as the solvent for the reduction measurements. The redox potentials are calculated relative to an internal reference ferrocenium/ferrocene ( $Cp_2Fe+/Cp_2Fe$ ). The UV-visible absorption spectra were measured by Hewlett-Packard 4853 diode array spectrophotometer. Singlet and triplet emission measurements were performed on a Photon Technology International QuantaMaster model C-60SE spectrofluorimeter at room temperature and 77 K.

#### 3.5. Device Fabrication

OLED devices were fabricated on pre-patterned ITO-coated glass substrates (20  $\pm$  5  $\Omega$ -cm², Thin Film Devices, Inc.). Prior to deposition, the substrates were cleaned with soap, rinsed with deionized water, and sonicated for 10 minutes. Afterwards, two subsequent rinses and 15-minute sonication baths were performed in acetone and isopropyl alcohol sequentially, followed by 10 min UV ozone exposure. EVO Vac 800 deposition system from Angstrom Engineering, at ~6 x 10-7 Torr. Current-voltage-luminescence (*J-V-L*) curves were measured in an inert atmosphere by using a Keithley power source meter model 2400 and a Newport multifunction optical model 1835-C, PIN-220DP/SB blue enhanced silicon photodiodes (OSI Optoelectronics Ltd.). Electroluminescence (EL) spectra of OLEDs were measured using the fluorimeter (Photon Technology International QuantaMaster model C-60SE) at several different voltages. Thicknesses were determined on Silicon wafers using a Filmsense FS-1 Ellipsometer.

#### 4. Summary

In this work, two spirobifluorenyl compounds, SB-C and SB-Si, were designed as host materials and analyzed for their chemical composition, optoelectronic properties, and performance in OLED devices. Both compounds have large HOMO/LUMO gaps (4.7  $\pm$  0.2 eV) and high triplet energies (2.8 eV). Despite their similarities, Hirshfeld surface

calculations and photophysical analysis of compounds in the solid-state crystals reveal that SB-Si displays more intermolecular C···C interactions than does SB-C. In both undoped devices and PHOLED devices, the SB-Si material demonstrated superior charge transporting abilities compared to the SB-C, as indicated by better current conduction and higher brightness. These findings illustrate the relationship between material morphology and properties, and their impact on charge transport in PHOLED devices. Furthermore, while triplet-triplet annihilation occurred in all SB-C doped devices, an external quantum efficiency of 10.2% was still achieved for its blue Ir(tpz)<sub>3</sub> device. The deleterious effects of dopant aggregation were effectively suppressed in the SB-Si devices, leading to high efficiencies for green Ir(ppy)<sub>3</sub> (EQE = 9.6%) and blue It(tpz)<sub>3</sub> (EQE = 12.6%) devices, with negligible roll-off below 40 mA/cm<sup>2</sup>. Overall, the results highlight the potential of SiPh<sub>3</sub> substituted spirobifluorenyl materials for use in PHOLED devices and underscore the importance of carefully considering material morphology and intermolecular interactions in optimizing device performance.

**Supplementary Materials:** The following supporting information can be downloaded at: www.mdpi.com/xxx/s1: electrochemical data, details of molecular modeling studies and OLED fabrication/testing results.

**Author Contributions:** Conceptualization, W.W., M.T.; data collection W.W., J.M., J.S., J.B., S.K., M.W.; writing, review and editing, W.W., J.M., P.D., M.T., J.S.

**Acknowledgements:** The authors wish to thank the Universal Display Corporation for funding this work. Part of the work presented here was taken from Dr. Wei's PhD thesis.[25]

**Conflicts of Interest:** One of the authors, Mark Thompson, has a financial interest in the Universal Display Corporation, the principal funding sources for this work.

References

- 1. Adachi, C.; Baldo, M.A.; Thompson, M.E.; Forrest, S.R. Nearly 100% internal phosphorescence efficiency in an organic light emitting device. *Journal of Applied Physics* **2001**, *90*, 5048-5051.
- 2. Kawamura, Y.; Goushi, K.; Brooks, J.; Brown, J.J.; Sasabe, H.; Adachi, C. 100% phosphorescence quantum efficiency of Ir(III) complexes in organic semiconductor films. *Appl. Phys. Lett.* **2005**, *86*, 071104.
- 3. Baldo, M.A.; O'Brien, D.F.; Thompson, M.E.; Forrest, S.R. Excitonic singlet-triplet ratio in a semiconducting organic thin film. *Physical Review B* **1999**, *60*, 14422.
- 4. Scholz, S.; Corten, C.; Walzer, K.; Kuckling, D.; Leo, K. Photochemical reactions in organic semiconductor thin films. *Org. Electron.* **2007**, *8*, 709-717, doi:DOI 10.1016/j.orgel.2007.06.002.
- 5. Scholz, S.; Walzer, K.; Leo, K. Analysis of complete organic semiconductor devices by laser desorption/ionization time-of-flight mass spectrometry. *Adv. Funct. Mater.* **2008**, *18*, 2541-2547, doi:DOI 10.1002/adfm.200700816.
- 6. Kondakov, D.Y.; Lenhart, W.C.; Nichols, W.F. Operational degradation of organic light-emitting diodes: Mechanism and identification of chemical products. *J. Appl. Phys.* **2007**, *101*, 024512, doi:10.1063/1.2430922.
- 7. Lin, W.C.; Wang, W.B.; Lin, Y.C.; Yu, B.Y.; Chen, Y.Y.; Hsu, M.F.; Jou, J.H.; Shyue, J.J. Migration of small molecules during the degradation of organic light-emitting diodes. *Org. Electron.* **2009**, *10*, 581-586, doi:DOI 10.1016/j.orgel.2009.02.012.
- 8. Sivasubramaniam, V.; Brodkorb, F.; Hanning, S.; Loebl, H.P.; van Elsbergen, V.; Boerner, H.; Scherf, U.; Kreyenschmidt, M. Fluorine cleavage of the light blue heteroleptic triplet emitter FIrpic. *Journal of Fluorine Chemistry* **2009**, *130*, 640-649, doi:10.1016/j.jfluchem.2009.04.009.
- 9. Holmes, R.J.; Forrest, S.R.; Tung, Y.J.; Kwong, R.C.; Brown, J.J.; Garon, S.; Thompson, M.E. Blue organic electrophosphorescence using exothermic host-guest energy transfer. *Appl. Phys. Lett.* **2003**, *82*, 2422-2424, doi:10.1063/1.1568146.

s 440 

4= 4

- 10. D'Andrade, B.W.; Forrest, S.R. Effects of exciton and charge confinement on the performance of white organic p-i-n electrophosphorescent emissive excimer devices. *J. Appl. Phys.* **2003**, *94*, 3101-3109.
- 11. O'Brien, D.F.; Baldo, M.A.; Thompson, M.E.; Forrest, S.R. Improved energy transfer in electrophosphorescent devices. *Appl.* 467 *Phys. Lett.* **1999**, 74, 442-444.
- 12. Baldo, M.A.; Lamansky, S.; Burrows, P.E.; Thompson, M.E.; Forrest, S.R. Very high-efficiency green organic light-emitting devices based on electrophosphorescence. *Appl. Phys. Lett.* **1999**, 75, 4-6.
- 13. Ren, X.F.; Li, J.; Holmes, R.J.; Djurovich, P.I.; Forrest, S.R.; Thompson, M.E. Ultrahigh energy gap hosts in deep blue organic electrophosphorescent devices. *Chem. Mater.* **2004**, *16*, 4743-4747, doi:10.1021/cm049402m.
- 14. Holmes, R.J.; D'Andrade, B.W.; Forrest, S.R.; Ren, X.; Li, J.; Thompson, M.E. Efficient, deep-blue organic electrophosphorescence by guest charge trapping. *Appl. Phys. Lett.* **2003**, *83*, 3818-3820, doi:10.1063/1.1624639.
- 15. Shih, P.I.; Chien, C.H.; Chuang, C.Y.; Shu, C.F.; Yang, C.H.; Chen, J.H.; Chi, Y. Novel host material for highly efficient blue phosphorescent OLEDs. *J. Mater. Chem.* **2007**, *17*, 1692-1698, doi:Doi 10.1039/B616043c.
- 16. Wei, W.; Djurovich, P.I.; Thompson, M.E. Properties of Fluorenyl Silanes in Organic Light Emitting Diodes. *Chem. Mat.* **2010**, 22, 1724.
- 17. Thiery, S.; Tondelier, D.; Declairieux, C.; Seo, G.; Geffroy, B.; Jeannin, O.; Rault-Berthelot, J.; Métivier, R.; Poriel, C. 9,9'-Spirobifluorene and 4-phenyl-9,9'-spirobifluorene: pure hydrocarbon small molecules as hosts for efficient green and blue PhOLEDs. *Journal of Materials Chemistry C* 2014, 2, 4156-4166, doi:10.1039/C4TC00171K.
- 18. Wong, K.-T.; Liao, Y.-L.; Lin, Y.-T.; Su, H.-C.; Wu, C.-c. Spiro-Configured Bifluorenes: Highly Efficient Emitter for UV Organic Light-Emitting Device and Host Material for Red Electrophosphorescence. *Org. Lett.* **2005**, *7*, 5131-5134, doi:10.1021/ol051865q.
- 19. Tian, G.; Jiang, Y.; Wu, P.; Huang, J.; Zou, Q.; Wang, Q.; Mu, H.; Su, J. Pure hydrocarbon host materials based on spirofluorene with excellent performances for green phosphorescent light-emitting devices. *New J. Chem.* **2016**, 40, 9500-9506, doi:10.1039/C6NJ01872F.
- 20. Jiang, Z.; Yao, H.; Zhang, Z.; Yang, C.; Liu, Z.; Tao, Y.; Qin, J.; Ma, D. Novel Oligo-9,9'-spirobifluorenes through ortho-Linkage as Full Hydrocarbon Host for Highly Efficient Phosphorescent OLEDs. *Org. Lett.* **2009**, *11*, 2607-2610, doi:10.1021/ol9008816.
- 21. Fan, C.; Chen, Y.; Gan, P.; Yang, C.; Zhong, C.; Qin, J.; Ma, D. Tri-, Tetra- and Pentamers of 9,9'-Spirobifluorenes through Full ortho-Linkage: High Triplet-Energy Pure Hydrocarbon Host for Blue Phosphorescent Emitter. *Org. Lett.* **2010**, *12*, 5648-5651, doi:10.1021/ol1024184.
- 22. Sicard, L.J.; Li, H.-C.; Wang, Q.; Liu, X.-Y.; Jeannin, O.; Rault-Berthelot, J.; Liao, L.-S.; Jiang, Z.-Q.; Poriel, C. C1-Linked

  Spirobifluorene Dimers: Pure Hydrocarbon Hosts for High-Performance Blue Phosphorescent OLEDs. *Angew. Chem. Int. Ed.*2019, 58, 3848-3853, doi:10.1002/anie.201813604.
- 23. Jeong, S.; Cho, S.; Lee, H.W.; Kim, Y.K.; Yoon, S.S. Triphenylsilane-Fluorene Hybrids as Host Materials for Green and Blue Phosphorescent Organic Light Emitting Diodes. *Journal of Nanoscience and Nanotechnology* **2017**, *17*, 5550-5555, doi:10.1166/jnn.2017.14113.
- 24. Kim, H.M.; Seo, J.H.; Lee, K.H.; Kang, H.J.; Yoon, S.S.; Kim, Y.K. Highly Efficient Phosphorescent Green Organic Light-Emitting Diodes with High Energy Gap Host Materials. *Mol. Cryst. Liq. Cryst.* 2010, 530, 83/[239]-290/[246], doi:10.1080/15421406.2010.495912.
- 25. Wei, W., **2010**. *High energy hosts and blue emitters for phosphorescent organic light emitting diodes.* [Doctoral Dissertation, 503 University of Southern California], (Publication No. 3434530) ProQuest Dissertations and Theses Global.
- 26. Spackman, M.A.; Jayatilaka, D. Hirshfeld surface analysis. *Crystengcomm* **2009**, *11*, 19-32, doi:10.1039/B818330A.

doi:10.1002/chem.200701036.

Optical Materials 2021, 9, 2001994, doi:10.1002/adom.202001994.

**1950**, 72, 4253-4255.

36.

37.

525

526

527

528

529

530

531

27.	Rault-Berthelot, J.; Granger, M.M.; Mattiello, L. Anodic oxidation of 9,9'-spirobifluorene in CH2Cl2 + 0.2 M Bu4NBF4.	506
	Electrochemical behaviour of the derived oxidation product. Synth. Met. 1998, 97, 211-215.	507
28.	Ye, S.H.; Liu, Y.Q.; Di, C.A.; Xi, H.X.; Wu, W.P.; Wen, Y.G.; Lu, K.; Du, C.Y.; Liu, Y.; Yu, G. Wide-Energy-Gap Host Materials	508
	for Blue Phosphorescent Organic Light-Emitting Diodes. Chem. Mater. 2009, 21, 1333-1342, doi:Doi 10.1021/Cm8032302.	509
29.	Wei, W.; Djurovich, P.I.; Thompson, M.E. Properties of Fluorenyl Silanes in Organic Light Emitting Diodes. Chem. Mater.	510
	<b>2010</b> , 22, 1724-1731, doi:10.1021/cm903146x.	511
30.	Sworakowski, J.; Lipiński, J.; Janus, K. On the reliability of determination of energies of HOMO and LUMO levels in organic	512
	semiconductors from electrochemical measurements. A simple picture based on the electrostatic model. Org. Electron. 2016,	513
	33, 300-310, doi:10.1016/j.orgel.2016.03.031.	514
31.	O'Brien, D.F.; Burrows, P.E.; Forrest, S.R.; Koene, B.E.; Loy, D.E.; Thompson, M.E. Hole transporting materials with high	515
	glass transition temperatures for use in organic light-emitting devices. Advanced Materials 1998, 10, 1108.	516
32.	$Koene, B.E.; Loy, D.E.; Thompson, M.E.\ Asymmetric\ triaryldiamines\ as\ thermally\ stable\ hole\ transporting\ layers\ for\ organic$	517
	light-emitting devices. Chem. Mater. 1998, 10, 2235-2250.	518
33.	Shirota, Y. Organic materials for electronic and optoelectronic devices. J. Mater. Chem. 2000, 10, 1-25.	519
34.	Shirota, Y. Photo- and electroactive amorphous molecular materials - molecular design, syntheses, reactions, properties,	520
	and applications. J. Mater. Chem. 2005, 15, 75-93.	521
35.	Poriel, C.; Liang, JJ.; Rault-Berthelot, J.; Barrière, F.; Cocherel, N.; Slawin, A.M.Z.; Horhant, D.; Virboul, M.; Alcaraz, G.;	522
	Audebrand, N.; et al. Dispirofluorene-Indenofluorene Derivatives as New Building Blocks for Blue Organic	523
	Electroluminescent Devices and Electroactive Polymers. Chemistry - A European Journal 2007, 13, 10055-10069,	524

Weisburger, J.H.; Weisburger, E.K.; Ray, F.E. Some derivatives of 9,9'-spirobifluorene. Journal of the American Chemical Society

Idris, M.; Kapper, S.C.; Tadle, A.C.; Batagoda, T.; Muthiah Ravinson, D.S.; Abimbola, O.; Djurovich, P.I.; Kim, J.; Coburn, C.;

Forrest, S.R.; et al. Blue Emissive fac/mer-Iridium (III) NHC Carbene Complexes and their Application in OLEDs. Advanced

## **Supporting Information**

### for

# A Comparison between Triphenylmethyl and Triphenylsilyl Spirobifluorenyl Hosts: Synthesis, Photophysics and Performance in Phosphorescent Organic Light-Emitting Diodes

Wei Wei <sup>1,†</sup>, Jie Ma <sup>2,†</sup>, Jonas Schaab <sup>1</sup>, Jason Brooks <sup>3</sup>, Seogshin Kang <sup>1</sup>, Matthew T. Whited <sup>1</sup>, Peter I. Djurovich <sup>1</sup> and Mark E. Thompson <sup>1,2,\*</sup>

- Department of Chemistry, University of Southern California, Los Angeles, CA 90089, USA
- Mork Family Department of Chemical Engineering and Materials Science, University of Southern California, Los Angeles, CA 90089, USA
- <sup>3</sup> Universal Display Corporation, Ewing, NJ 08618, USA
- \* Correspondence: met@usc.edu
- † These authors contributed equally to this work.

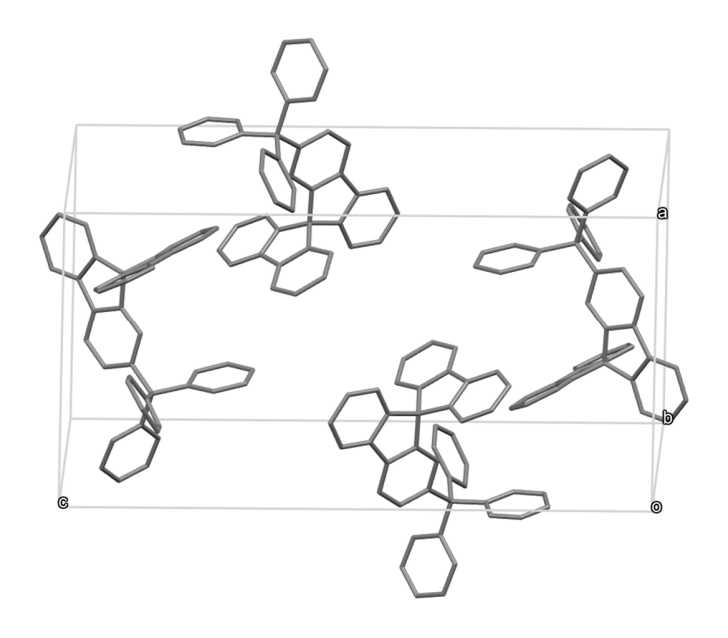
## Table of Contents

Table of Contents	1
Table S1: Crystallographic Data for SB-C and SB-Si	3
Figure S1. Packing of SB-C (top) and SB-Si (bottom) molecules in a unit cell	4
Figure S2. Calculated Hirshfeld surfaces of <b>SB-C</b> and <b>SB-Si</b> , which are shown in different viewing angles (front, left and back)	5
Figure S3. DFT calculated HOMO (solid) and LUMO (mesh) surface and levels of <b>SB-C</b> and <b>SB-Si</b> . Calculated values are compared to the measured values.	6
Figure S4. (a) Cyclic voltammetry curves of <b>SB-Si</b> and <b>SB-C</b> . (b) Differential pulse voltammetry curve of <b>SB-Si</b> and <b>SB-C</b> .	es 7
Figure S5. Differential scanning calorimetric (DSC) thermograms of <b>SB-Si</b> and <b>SB-C</b>	8
Figure S6. Voltage dependence of EL spectra of the undoped devices.	9

Table S1: Crystallographic Data for SB-C and SB-Si.

<b>Identification Code</b>	SB-C	SB-Si
Empirical formula	C44H30	C43H30Si
Formula weight	558.68	574.76
Temperature/K	101(1)	102(2)
Crystal system	Monoclinic	monoclinic
Space group	P2 <sub>1</sub> /n	P2 <sub>1</sub> /n
a/Å	13.2736(3)	13.54470(12)
b/Å	9.03871(19)	9.29422(8)
c/Å	24.5142(6)	24.5334(2)
α/°	90	90
β/°	91.929(2)	91.1600(8)
γ/°	90	90
Volume/Å <sup>3</sup>	2939.45(11)	3087.81(5)
Z	4	4
ρ <sub>cale</sub> g/cm <sup>3</sup>	1.262	1.236
$\mu/\text{mm}^1$	0.541	0.888
F(000)	1176.0	1208.0
Crystal size/mm <sup>3</sup>	$0.164 \times 0.11 \times 0.039$	$0.576 \times 0.201 \times 0.1$
Radiation	Cu K $\alpha$ ( $\lambda = 1.54184$ )	Cu K $\alpha$ ( $\lambda = 1.54184$ )
2Θ range for data collection/°	7.216 to 160.454	7.208 to 160.704
Index ranges	$-16 \le h \le 16, -11 \le k \le 7,$ $-31 \le 1 \le 30$	$-17 \le h \le 16, -8 \le k \le 11,$ $-31 \le 1 \le 31$
Reflections collected	23585	49890
Independent reflections	6180	6740
-	$[R_{int} = 0.0386, R_{sigma} = 0.0349]$	$[R_{int} = 0.0498, R_{sigma} = 0.0289]$
Data/restraints/parameters	6180/0/398	6740/0/398
Goodness-of-fit on F <sup>2</sup>	1.051	1.057
Final R indexes [I>= $2\sigma$ (I)]	$R_1 = 0.0408, wR_2 = 0.1035$	$R_1 = 0.0390, wR_2 = 0.1011$
Final R indexes [all data]	$R_1 = 0.0489$ , $wR_2 = 0.1078$	$R_1 = 0.0418$ , $wR_2 = 0.1032$
Largest diff. peak/hole/e Å <sup>-3</sup>	0.30/-0.21	0.45/-0.35
#CCDC	2221201	2216982

## SB-C Unit Cell



SB-Si Unit Cell

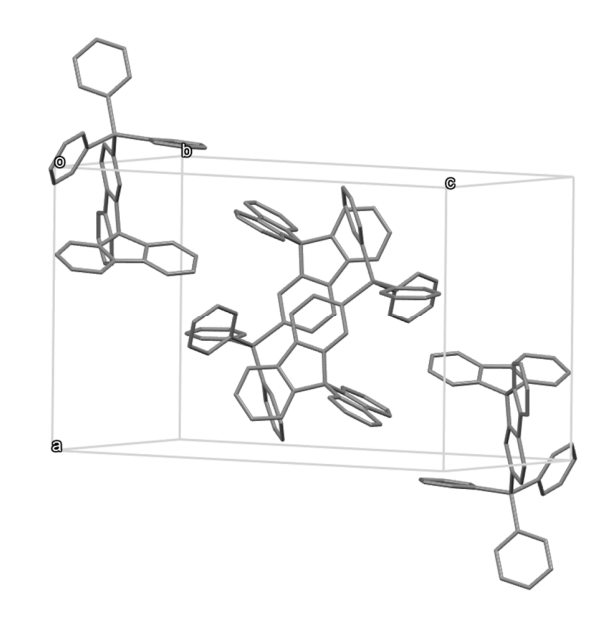


Figure S1. Packing of  ${\bf SB-C}$  (top) and  ${\bf SB-Si}$  (bottom) molecules in a unit cell.

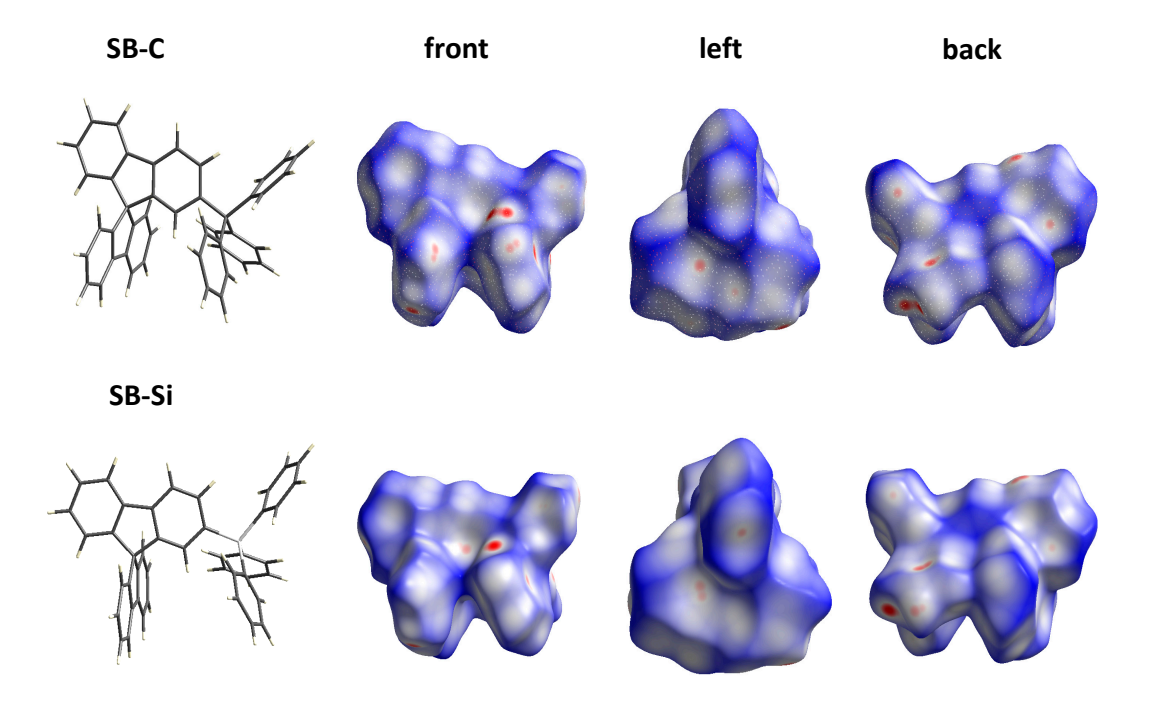


Figure S2. Calculated Hirshfeld surfaces of **SB-C** and **SB-Si**, which are shown in different viewing angles (front, left and back).

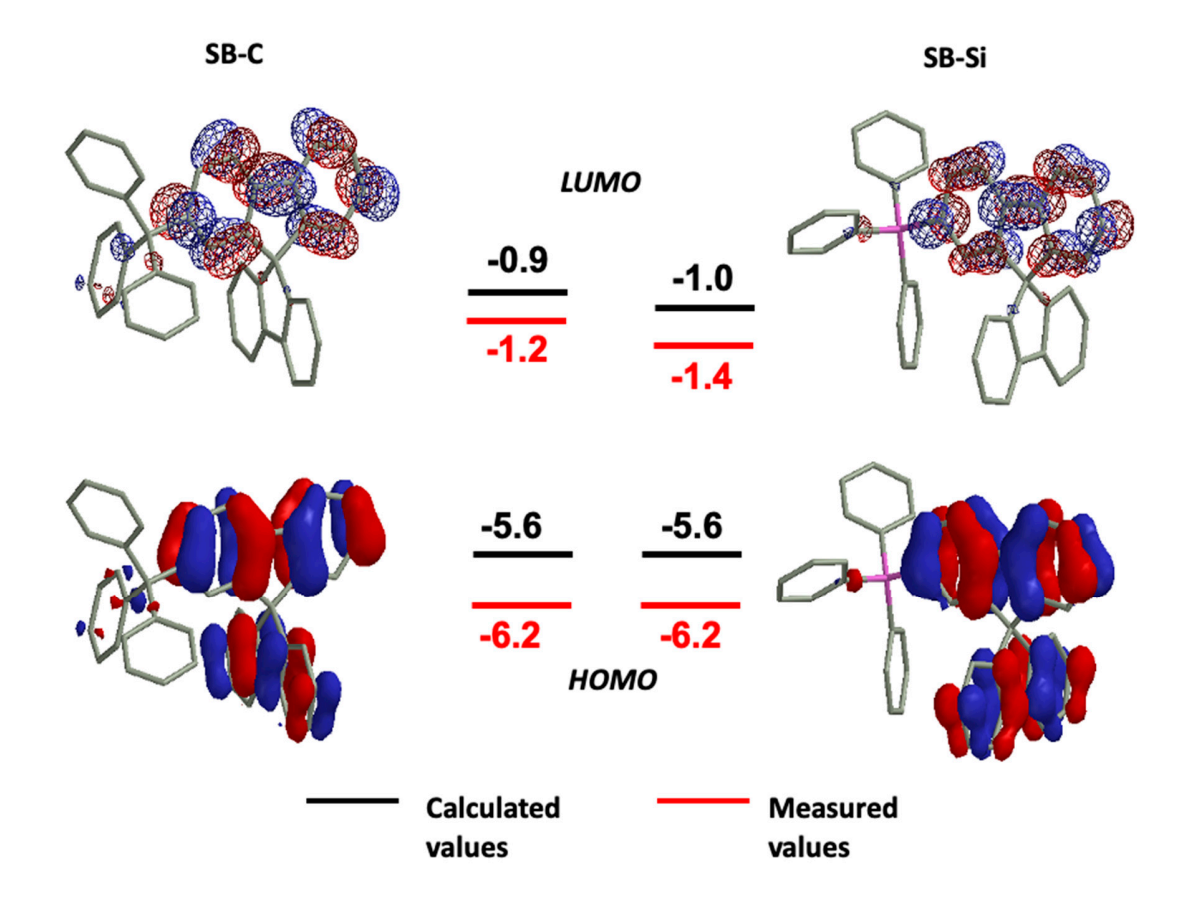
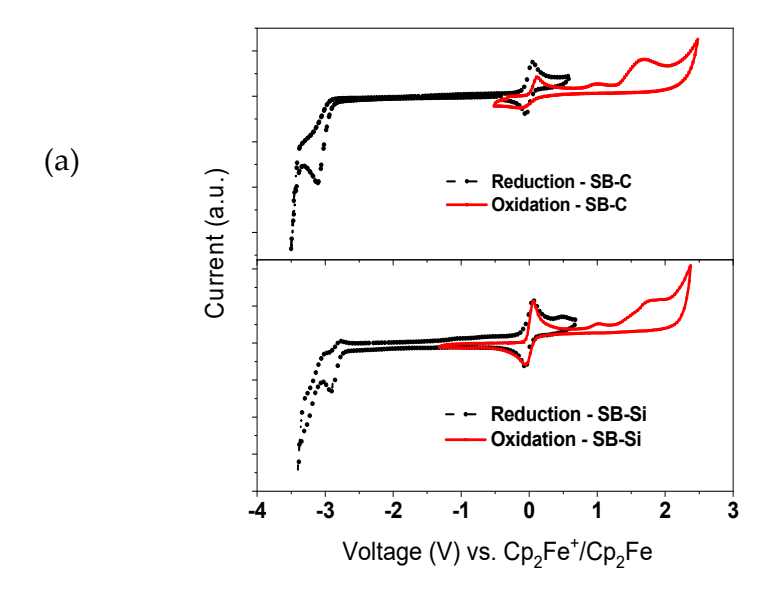


Figure S3. DFT calculated HOMO (solid) and LUMO (mesh) surface and levels of **SB-C** and **SB-Si**. Calculated values are compared to the measured values.



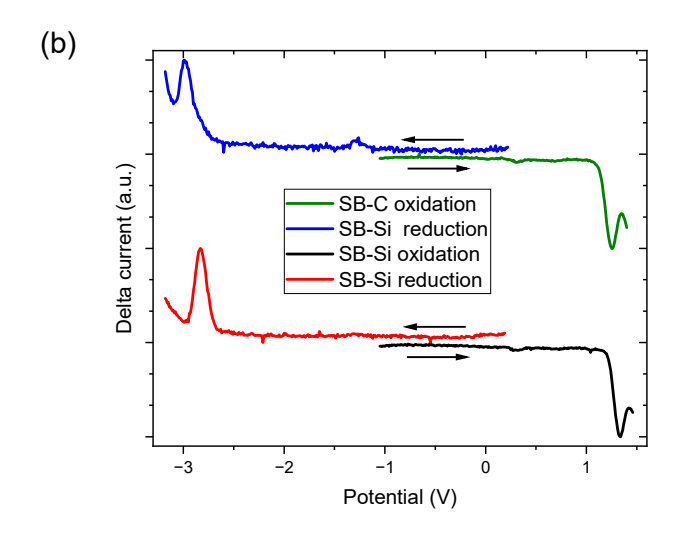


Figure S4. (a) Cyclic voltammetry and differential pulse voltammetry, (b), curves for SB-Si and SB-C.

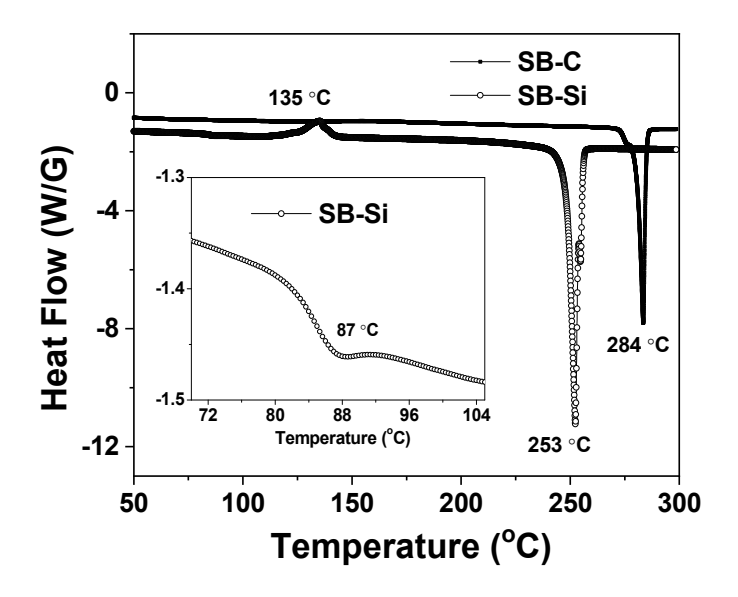
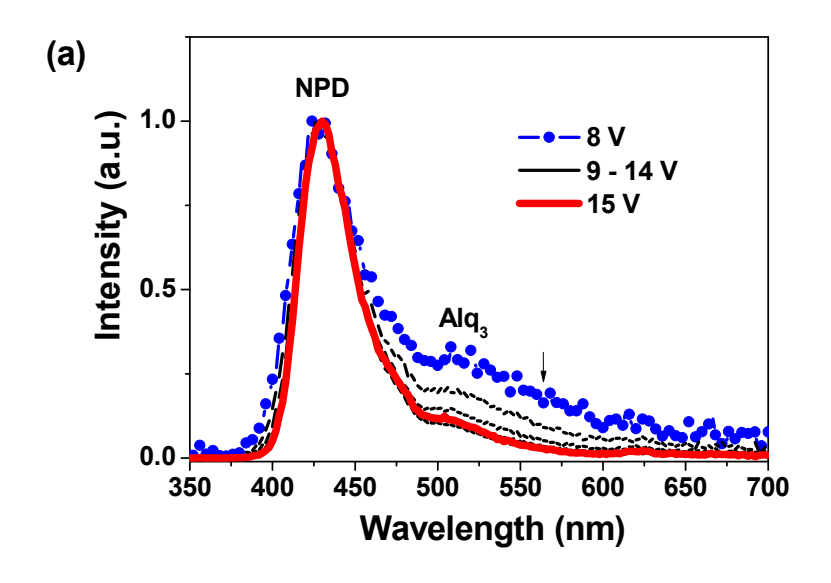


Figure S5. Differential scanning calorimetric (DSC) thermograms of **SB-Si** and **SB-C.** 



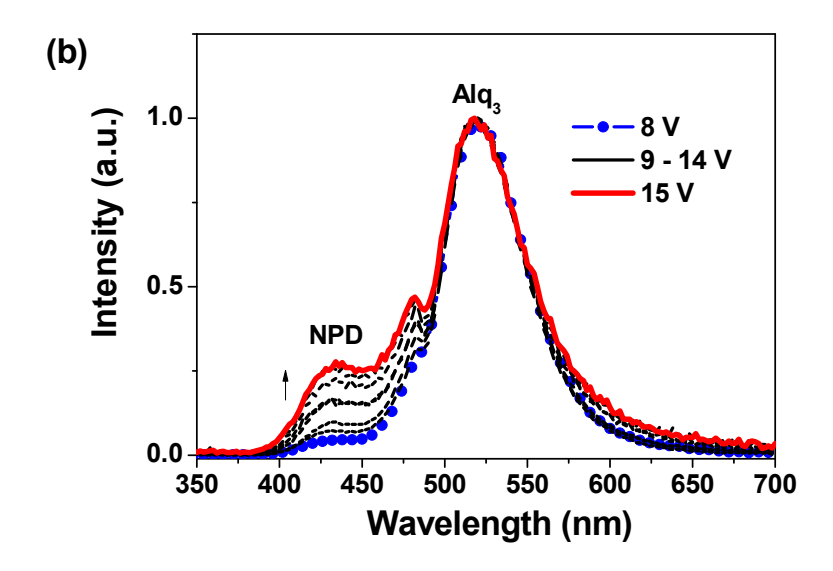


Figure S6. (a,b) Voltage dependence of EL spectra of the undoped devices.